Structural and functional properties of ryanodine receptor type 3 in zebrafish tail muscle

Stefano Perni,[1] Kurt C. Marsden,[1] Matias Escobar,[1] Stephen Hollingworth,[2] Stephen M. Baylor,[2] and Clara Franzini-Armstrong[1]

[1]Department of Cell and Developmental Biology and [2]Department of Physiology, University of Pennsylvania School of Medicine, Philadelphia, PA 19104

The ryanodine receptor (RyR)1 isoform of the sarcoplasmic reticulum (SR) Ca^{2+} release channel is an essential component of all skeletal muscle fibers. RyR1s are detectable as "junctional feet" (JF) in the gap between the SR and the plasmalemma or T-tubules, and they are required for excitation–contraction (EC) coupling and differentiation. A second isoform, RyR3, does not sustain EC coupling and differentiation in the absence of RyR1 and is expressed at highly variable levels. Anatomically, RyR3 expression correlates with the presence of parajunctional feet (PJF), which are located on the sides of the SR junctional cisternae in an arrangement found only in fibers expressing RyR3. In frog muscle fibers, the presence of RyR3 and PJF correlates with the occurrence of Ca^{2+} sparks, which are elementary SR Ca^{2+} release events of the EC coupling machinery. Here, we explored the structural and functional roles of RyR3 by injecting zebrafish (*Danio rerio*) one-cell stage embryos with a morpholino designed to specifically silence RyR3 expression. In zebrafish larvae at 72 h postfertilization, fast-twitch fibers from wild-type (WT) tail muscles had abundant PJF. Silencing resulted in a drop of the PJF/JF ratio, from 0.79 in WT fibers to 0.03 in the morphants. The frequency with which Ca^{2+} sparks were detected dropped correspondingly, from 0.083 to 0.001 sarcomere^{-1} s^{-1}. The few Ca^{2+} sparks detected in morphant fibers were smaller in amplitude, duration, and spatial extent compared with those in WT fibers. Despite the almost complete disappearance of PJF and Ca^{2+} sparks in morphant fibers, these fibers looked structurally normal and the swimming behavior of the larvae was not affected. This paper provides important evidence that RyR3 is the main constituent of the PJF and is the main contributor to the SR Ca^{2+} flux underlying Ca^{2+} sparks detected in fully differentiated frog and fish fibers.

The Journal of General Physiology

INTRODUCTION

Excitation–contraction (EC) coupling refers to a series of steps in muscle fibers that links depolarization of the plasmalemma to contraction. In all skeletal muscles, from fish to mammals, the step that initiates Ca^{2+} release from the SR involves a stereospecific protein–protein interaction between calcium channels of the surface membrane or T-tubules, $Ca_V1.1$ (or dihydropyridine receptors [DHPRs]) acting as voltage sensors, and calcium release channels of the SR (or RyRs) whose cytoplasmic domains constitute the "feet" identified in electron micrographs (EMs) (Block et al., 1988; Lai et al., 1988). The coupling events take place within calcium release units (CRUs), including triads, dyads, and peripheral couplings, where the unique interaction between DHPR and RyR channels (Nakai et al., 1996) organizes the DHPRs into RyR-associated tetrads (Protasi et al., 1998). Of the three known RyR isoforms in vertebrates, only RyR1 (sometimes referred to as "RyRα" in lower vertebrates) is present in all skeletal muscles and is an essential structural and functional component therein. The absence of RyR1, caused by either spontaneous or engineered mutations, results in muscle paralysis and highly defective differentiation of the fibers (Takeshima et al., 1994; Ivanenko et al., 1995; Takekura et al., 1995; Moore et al., 1998).

Most skeletal muscle fibers express a second isoform, RyR3 (sometimes referred to as "RyRβ" in lower vertebrates) (Airey et al., 1990; Hakamata et al., 1992; Murayama and Ogawa, 1992; Percival et al., 1994), but its expression level differs greatly among different fiber types. The RyR3/RyR1 ratio is 0 in superfast fibers of toadfish swimbladder (O'Brien et al., 1993), very low in adult mammalian muscles (Giannini et al., 1995), but close to 1 in tail muscles of toadfish and some twitch fibers of birds and amphibians (Airey et al., 1990; Murayama and Ogawa, 1992). This difference in RyR3 expression is correlated with a significant anatomical difference. All muscles contain arrays of regularly disposed feet in the gap between the junctional SR (JSR) and T-tubules and, in

Correspondence to Stefano Perni: stefano.perni@ucdenver.edu

S. Perni's present address is Dept. of Physiology and Biophysics, University of Colorado, Anschutz Medical Campus, Aurora CO, 80045.

Abbreviations used in this paper: CRU, calcium release unit; DHPR, dihydropyridine receptor; EC, excitation–contraction; EM, electron micrograph; hpf, hours postfertilization; JF, junctional feet; JSR, junctional SR; MO, morpholino; PJF, parajunctional feet.

The Rockefeller University Press $30.00
J. Gen. Physiol. Vol. 145 No. 3 173–184
www.jgp.org/cgi/doi/10.1085/jgp.201411303

fibers lacking RyR3, it is clear that these junctional feet (JF) are constituted of RyR1. In fibers expressing RyR3, however, an additional set of feet—the parajunctional feet (PJF)—is seen, located in the triads at the sides of the SR membrane immediately adjacent to the gap between the JSR and the T-tubule but facing toward the myofibrils rather than toward the T-tubules (Felder and Franzini-Armstrong, 2002). Based on the correlation between RyR3 and PJF content, these authors proposed that PJF are in fact RyR3 proteins relegated to the sides of the triads. Because PJF are not directly apposed by DHPRs, the authors also proposed that (a) the release of Ca^{2+} from RyR3 must depend on a mechanism other than a protein–protein interaction with DHPRs, for instance on Ca^{2+}-induced Ca^{2+} release (CICR); and (b) the role of RyR3 during EC coupling might be to amplify, through CICR, the release of Ca^{2+} initiated by RyR1 (see also O'Brien et al., 1993, Klein et al., 1996, and Shirokova et al., 1998). Importantly, RyR3, in contrast to RyR1, cannot, by itself, sustain the usual functional and structural roles essential to EC coupling, even though RyR3 can become an integral part of CRUs (Protasi et al., 2000).

Evidence concerning the differing functions of RyR1 versus RyR3 has also been observed with single-channel current measurements in bilayer experiments, where RyR3 reveals a higher open probability when activated by Ca^{2+} and less susceptibility to inactivation at high concentrations of Ca^{2+} (e.g., O'Brien et al., 1993; Ogawa et al., 2000). This result has been interpreted to indicate that RyR3 may play a preferred role in physiological processes involving CICR in skeletal muscle and some other tissues.

A distinct role for the two RyR isoforms during EC coupling is also suggested by measurements with the fluorescent Ca^{2+} indicators fluo-3 or fluo-4 introduced into the myoplasm of functioning skeletal muscle fibers. Such fibers, when studied with confocal microscopy, can, in some circumstances, reveal small, highly localized fluorescence changes, termed "Ca^{2+} sparks," that are reflective of localized increases in myoplasmic [Ca^{2+}] caused by SR Ca^{2+} release by a small number of active RyRs (Tsugorka et al., 1995; Klein et al., 1996; Hollingworth et al., 2001). Importantly, Ca^{2+} sparks were detected during voltage-clamp depolarizations of adult frog fibers, which contain both RyR1 and RyR3, but not of adult rat fibers, which contain only RyR1 (Shirokova et al., 1998). Under other experimental conditions, small localized SR Ca^{2+} release events (also generically called "Ca^{2+} sparks") have been detected in confocal studies of embryonic, neonatal, and adult rodent fibers, as well as myogenic cell lines (Conklin et al., 1999, 2000; Shirokova et al., 1999; Kirsch et al., 2001; Ward et al., 2001; Wang et al., 2005). Although these studies indicate that local Ca^{2+} release events can be detected in fibers that exclusively express either the RyR1 or the RyR3 isoform, the morphological properties of these events are typically highly variable and/or the events are not under voltage control. Thus, these Ca^{2+} sparks usually differ substantially from those of the spontaneous and/or voltage-induced Ca^{2+} sparks that likely arise from activity of the EC-coupling machinery in normally functioning adult fibers. The latter type of Ca release events have, to date, only been reported in fibers that normally express both RyR1 and RyR3 (Klein et al., 1996; Shirokova et al., 1998; Hollingworth et al., 2001) and are not found in fibers that express only RyR1 (Shirokova et al., 1998).

The aim of inducing frog-type Ca^{2+} spark behavior in (adult) mouse fibers by the overexpression of RyR3 was attempted by Pouvreau et al. (2007) in flexor digitorum brevis muscles. Spontaneous and voltage-activated Ca^{2+} sparks were observed in the overexpressing fibers; however, the RyR3/RyR1 ratio could not be finely controlled and, although the exogenous RyR3 was targeted in close proximity to the triads, the location of the feet could not be ascertained. Another study with a similar aim was unsuccessful in revealing Ca^{2+} sparks (Legrand et al., 2008).

The work presented here, which investigates the role of RyR3 in SR Ca^{2+} release in the tail muscles of zebrafish larvae, is based on the initial observations that (a) muscle fibers in the tail myotomes of zebrafish have fully differentiated triads as early as 48 to 72 hours postfertilization (hpf) and (b) the triads in the fast-twitch fibers that constitute the bulk of the tail muscles contain arrays of PJF that are quite similar to those found in frog fibers. We were therefore interested to see if these zebrafish fibers have readily detectable Ca^{2+} sparks that depend on the presence of the RyR3 isoform. Our experimental approach used the well-established procedure for silencing specific protein expression in these small fish by injecting mRNA inhibitory molecules in the one-cell stage embryos. Tail myotomes in zebrafish larvae thereby offer the unique opportunity of comparing, in the same species, structural and functional effects of having a full complement of RyR3 versus a greatly reduced level of expression of RyR3.

MATERIALS AND METHODS

Animals and larvae manipulation

WT Tubingen strain zebrafish (*Danio rerio*) were mated and the embryos were used either uninjected or injected, at the one-cell stage, with a morpholino (MO) solution. The larvae were grown for 72 h in E3 medium (mM: 5 NaCl, 0.17 KCl, 0.33 $CaCl_2$, and 0.33 $MgSO_4$).

Protein expression silencing

An RyR3-mRNA splice-blocking MO, based on a 25-nucleotide (5′-GAGCGGCGTTTTTACTTACAGTCCG-3′) Zebrafish Model Organism Database (ZFIN) sequence (ZFIN ID: ZDB-MRPHLNO-090109-2), was obtained from GeneTools. The MO is designed to specifically pair with the first exon splice junction of RyR3 mRNA,

thus impairing the protein translation. We used a 3-mM MO stock solution diluted at 1:12 in Danieau's solution (mM: 58 NaCl, 0.7 KCl, 0.4 $MgSO_4$, 0.6 $Ca(NO_3)_2$, and 5 HEPES plus phenol red). A droplet of this solution with a diameter of ∼0.09 mm was used for injection into the oocyte. Two sets of fish were used as controls: uninjected WT larvae and larvae injected with an unrelated MO (tbx5; provided by W. Talbot, Stanford University School of Medicine, Stanford, CA) in the same Danieau's solution. The second control was designed to block the Tbx5 protein, which is important in vertebrate limb development (Tamura et al., 1999), allowing us to easily test the efficiency and specificity of the injection by verifying the absence of pectoral fins in morphant larvae (see Fig. S2) and the unaffected presence of PJF.

Electron microscopy

Tails were fixed in 4–6% glutaraldehyde buffered with 0.1 M sodium cacodylate, pH 7.2–7.4, post-fixed in 2% OsO_4 in the same buffer for 1 h at 4°C, en bloc stained with a saturated solution of uranyl acetate in H_2O, and embedded in epon. Thin sections were stained with lead acetate for contrast and examined in an electron microscope (Philips 410; Philips Electron Optics). The images were digitally recorded with a digital camera (Hamamatsu C4742-95; Advanced Microscopy Techniques).

PJF/JF ratios were calculated by direct counting in EM images of triads in longitudinal sections. The images used for the analysis of feet were obtained following a strictly random approach: for each larva (7 WT and 10 morphants; see Table 1, described in Results), the first 10 fiber segments that appeared on the screen and were in good longitudinal orientation were used; in each fiber, all triads that were appropriately oriented in the section were digitally recorded. The orientation of triads in the sections was independent of the operator, thus constituting a nonbiased collection of images. The counting of JF and PJF was done by Clara Franzini-Armstrong, the most experienced electron microscopist in the group. Automated image analysis was not used because of (a) the difficulty of establishing a reference by which a sub-image window containing the appropriate region of a triad could be routinely identified (for instance, the position of triads at the level of the Z-line and the size and shape of the T-tubules are sufficiently variable that they cannot be easily used for automated image selection); and (b) the difficulty of developing algorithms to differentiate between variations in a sub-image caused by the absence or presence of PJF versus variations caused by slight distortions of the triad membrane profiles, minor variations in the angles at which the triads are seen, and differing electron optical densities of the feet. Because of these same issues, our visual counting of PJF may involve some minor error in the estimate of PJF frequency, which we doubt could exceed 10% (for example, see Fig. 3, described in Results). In general, we tried to be generous in assigning foot identification in the case of morphant fibers. The structural differences between WT and morphant triads regarding JF and PJF numbers were so striking, to both trained and untrained observers, that further approaches, such as full counting by multiple observers, was considered unnecessary.

Single fiber isolation

72 hpf larvae were anesthetized using 0.03% tricaine methanesulfonate (MS-222; Spectrum Chemical) in E3 medium. After decapitation, the distal, less developed, approximately one-third portion of the tail was cut away and 20–50 proximal tails were washed in ice-cold 0.5× Hank's balanced salt solution (HBSS). The proximal tails were digested in 200 U/ml collagenase (from *Clostridium histolyticum*; Sigma-Aldrich) in 1× HBSS for ≈1.5 h (or until no trace of tails was visible) under agitation at 28°C and trituration every 15 min with a fine-tip plastic transfer pipette. Digestion was stopped by adding 10 volumes of culture medium (60% L-15, 3% fetal bovine serum, 3% horse serum, 4 mM glutamine, and penicillin/streptomycin). The fibers were pelleted by centrifugation (200 *g* for 5 min) and resuspended in a minimum of 200 µl of culture medium. Fibers were then plated on a Matrigel (Corning)-coated glass coverslip inside a 35-mm culture dish. After 15 min, 1.5 ml of culture medium was added. Fibers were incubated for at least 1 h at 28°C before calcium imaging.

Calcium signal detection and analysis

Myocytes on a Matrigel-coated coverslip were AM loaded with the Ca^{2+} indicator fluo-4 (Life Technologies) for ∼30 min at room temperature (∼23°C) in a bathing solution (mM): 140 NaCl, 2.8 KCl, 2.0 $CaCl_2$, 2 glucose, and 10 HEPES, pH 7.3. The fluo-4 AM concentration was 10 µM with 0.2% DMSO and 0.02% wt/vol pluronic. Loaded fibers were transferred to a home-built confocal microscope (Hollingworth et al., 2001) and imaged at 18°C in the bathing solution with 0.3 mM caffeine to stimulate SR calcium release. Results are reported from four different experiments, in each of which a WT and a morphant preparation, both 72 hpf, were imaged on the same afternoon; ∼10 fibers were imaged from each preparation per experiment. Ca^{2+} sparks were detected in X-T line scans and analyzed as described previously (Hollingworth et al., 2001, 2006). To maximize the number of fibers from which spark frequency could be estimated, raw images, in which the time-averaged fluorescence intensity per pixel (F) was ≥2 photons/µs, were converted to ΔF/F images and filtered with 3 × 3 rectangular smoothing for spark detection. Spark frequencies are reported from fibers in which at least 100 sarcomere × seconds of imaging above 2 photons/µs were completed. In a subset of images from some of these fibers, the time-averaged pixel intensity was ≥4.5 photons/µs and smaller Ca^{2+} sparks could be reliably detected. Temporal and spatial profiles of the sparks detected in these images were obtained from the unsmoothed ΔF/F images and fitted with standard waveforms (Lacampagne et al., 1999; Hollingworth et al., 2001, 2006). Fitted spark properties were considered reliable if the fitted ΔF/F amplitude was ≥0.5 (Hollingworth et al., 2006). The ΔF/F amplitude and spark mass obtained from WT sparks were scaled by 1.1 to enable a better comparison with morphant spark properties. This scaling is required because F in the WT fibers will be higher than that in morphant fibers because of the increased sparking activity in the WT fibers. The 1.1 factor is an empirical factor based on experiments in intact frog fibers (Fig. 8 in Hollingworth et al., 2006) and the averaged spark frequencies observed in the WT and morphant myocytes.

Swimming behavior analysis

MO-injected and uninjected sibling larvae at 72 hpf were mounted dorsally in 2% agarose dissolved in E3 in individual 35-mm imaging dishes. Tails were freed by cutting away agarose distal to the yolk, leaving the heads fully restrained. For behavior imaging, a 96-bulb infrared LED array (IR100 Illuminator removed from its housing; YYTrade) was positioned below a 3-mm-thick sheet of white acrylic to diffuse the IR light. Dishes were placed directly on the acrylic sheet. A white LED bulb (PAR38 LED light; LEDlight.com) was positioned above the testing area to provide white-light illumination. Bouts of swimming were induced by gently touching the distal tail with a handheld nylon filament. High speed video images at 1,000 frames/s and 512 × 512–pixel resolution were recorded using a camera (Motionpro; Redlake) with a 50-mm macro lens. Behavioral analysis was performed with the FLOTE software package (Burgess and Granato, 2007a,b; Burgess et al., 2009; Wolman et al., 2011). Tail curvature was calculated by dividing the body of each larva into four segments and summing the angles between segments 2 and 3 and segments 3 and 4.

Statistical analysis

Statistical tests were performed with Student's two-tailed *t* test. Results were considered significant if $P < 0.01$.

Online supplemental material

Fig. S1 reports the Western blotting analysis of the expression of RyR1 and RyR3, showing the disappearance of one of the three bands revealed by the pan anti-RyR antibody 34C and the appearance of a new band at smaller MW (truncated protein) in the MO. Zebrafish, like other teleost fish, express two paralogous copies of RyR1 (RyR1a and RyR1b) (Franck et al., 1998; Darbandi and Franck, 2009), thus explaining the presence of three bands instead of two. Fig. S2 shows the effects of tbx5-MO in injected larvae. Successfully injected larvae lack pectoral fins, but the distribution of PJF is unaffected. The online supplemental material is available at http://www.jgp.org/cgi/content/full/jgp.201411303/DC1.

RESULTS

72 hpf zebrafish larvae have fully differentiated and ordered muscle fibers, revealing the presence of PJF

At 3 d after fertilization, zebrafish larvae show fully differentiated and ordered muscle fibers within myotomes of the proximal tail segments. T-tubules are transversally oriented, are located at the Z-line, and are flanked by the JSR-terminal cisternae to form classical triads. In fast-twitch fibers, which comprise the bulk of the tail, JSR contains a limited amount of calsequestrin (Fig. 1, A and B). In the slow-twitch fibers (not depicted), which are located in a single layer along the edges of the tail (Devoto et al., 1996; Elworthy et al., 2008), calsequestrin is more abundant.

In cross sections and in longitudinal sections at higher magnification, triads in the fast fibers reveal two distinct sets of RyRs (whose cytoplasmic domains are visible as feet). One set of feet, the JF, is organized in two parallel rows located in the narrow gap where the membranes of JSR and T-tubules face each other (Fig. 1, B and C, arrowheads). The other set of feet, the parajunctional ones (PJF), is located in proximity of the junction but on the side of the JSR cisternae facing the myofibrils (Fig. 1, B and C, arrows). In cross sections of the fiber (Fig. 2, A and B), it is clear that the two continuous rows of JF (outlined in yellow in B) are accompanied on each side by discontinuous rows of PJF (outlined in light purple in B), which may be either single or double (see double arrows in Fig. 1 B). Both JF and PJF make contact within the homologous rows, but a small but quite distinct gap separates JF from PJF. A modified copy of the cartoon model (Felder and Franzini-Armstrong, 2002) illustrating this arrangement and showing that JF

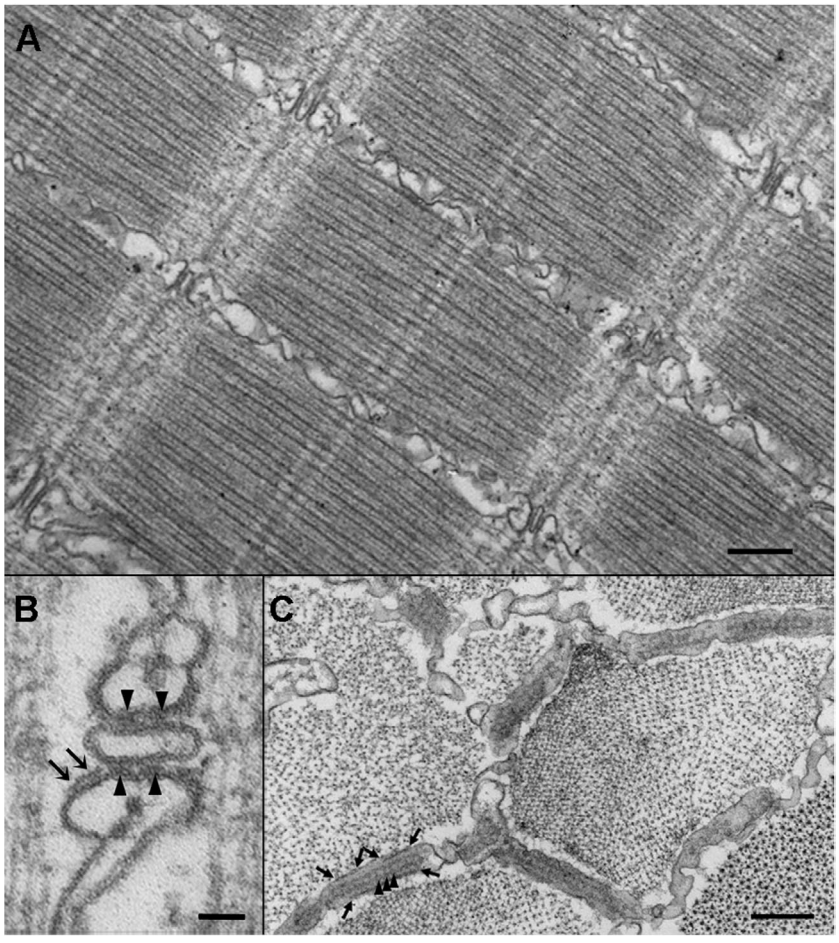

Figure 1. Images from thin sections of tail myotomes from 72 hpf larvae. (A) Detail of a muscle fiber in a 72 hpf larva. At this age, fibers in proximal myotomes have well-differentiated myofibrils and CRUs in the form of triads located at the Z-line. Bar, 250 nm. (B) Triads in fast-twitch fibers, constituting the majority of the tail, have two sets of "feet": JF located between SR and T-tubule membranes (arrowheads), and PJF located near the junction but on the side of the SR facing the myofibrils (arrows). Bar, 50 nm. (C) Cross sections of the fibers offer grazing views of the junctional gap, occupied by two rows of JF (arrowheads) and two other discontinuous rows of PJF (delimited by the arrows) on the side of the SR cisterna. Bar, 250 nm.

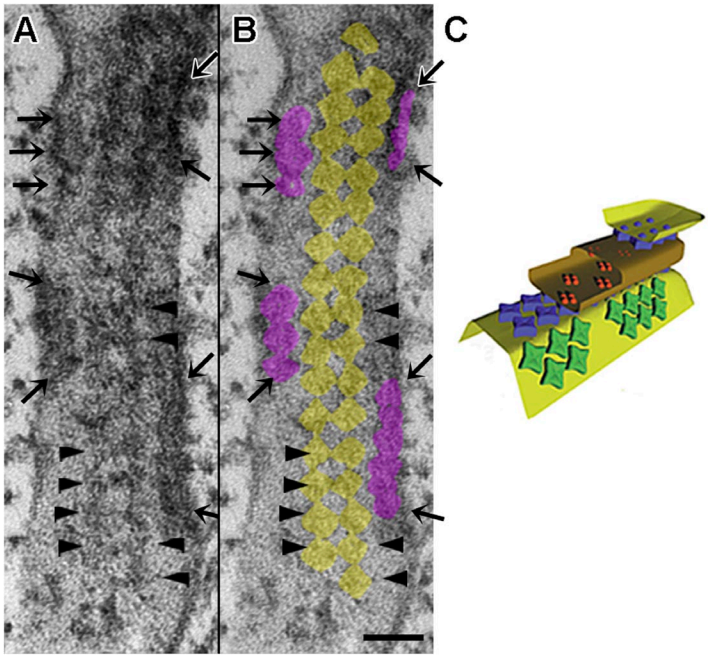

Figure 2. Differences in the JF and PJF arrays. (A and B) Original and highlighted versions of the junctional gap indicated by arrows in Fig. 1 C. The two continuous rows of JF are lined on either side by discontinuous rows of PJF, highlighted in yellow and in light purple, respectively in B. Note that feet contact each other within the rows, but PJF and JF are separated by a gap. Bar, 50 nm. Arrowheads identify JF, horizontal arrows identify PJF, and angled arrows delimit discontinuous rows of PJF. (C) A revised version of an illustration in Felder and Franzini-Armstrong (2002) showing a 3-D model of a triad with JF in blue and PJF in green.

and PJF establish different relationships with each other is shown in Fig. 2 C.

The slow-twitch fibers show only JF (not depicted), in accordance with the in situ hybridization and immunolabeling data from Wu et al. (2011). Because the relative frequency of these fibers at 72 hpf is very small, they were ignored in the rest of the project.

Silencing of RyR3 expression results in virtual absence of the PJF

Thin sections of fast-twitch fibers from 72 hpf morphant larvae show no signs of muscle degeneration or disarrangement compared with WT (Fig. 3, A and C). This result is not surprising, as the larvae did not show any obvious development abnormalities (Fig. 3, A and C, insets). However, a major anatomical alteration is the essentially complete absence of PJF in MO-injected tails versus WT (Fig. 3, B and D). For both samples, triads are shown as simple images (top) and after enhancing the position of JF in yellow and PJF in purple (bottom). All triads show two JF profiles on each side of the T-tubule. The great majority of WT triads show one or two PJF in at least one of the four parajunctional positions of the two JSR cisternae (Fig. 3 B), but PJF are absent in practically all the triads of MO-treated tails (Fig. 3 D). The triad at right in Fig. 3 D shows one of the very rare triads in which PJF are present. Extensive counts from a large number of triads in 7–10 fish indicate that the ratio of PJF to JF is 0.79 ± 0.14 (mean ± SD; $n = 7$) in WT triads and 0.03 ± 0.03 ($n = 10$) in MO-treated fibers (Table 1). The 0.79 ratio we found in WT larvae is essentially in agreement with the range of 0.77–0.64 in adult fish calculated using qRT-PCR (Darbandi and Franck, 2009), considering that the expression of RyR1a and RyR1b, but not RyR3, is noticeably lower in the 72 hpf larva than in the adult (see Fig. 3 A in Wu et al., 2011). The effects of the MO on RyR3 expression are also confirmed by Western blotting analysis (Fig. S1).

MO-tbx5 larvae showed the lack of fins to be expected from down-regulation of the Tbx5 protein, but PJF were fully present. This confirmed that the almost complete disappearance of PJF was directly related to the injection of the specific MO designed to disrupt expression of RyR3 (see Fig. S2).

RyR3 silencing causes a dramatic reduction of readily detectable spontaneous calcium sparks in isolated fast-twitch fibers from zebrafish larvae

To investigate whether the relative absence of RyR3 and of PJF influences the ability of fibers to generate Ca^{2+} sparks, myocytes isolated from 72 hpf WT and morphant larvae were loaded with fluo-4 AM and imaged on a confocal microscope. The bathing solution included 0.3 mM caffeine to stimulate SR Ca^{2+} release. Fig. 4 A shows typical X-Y images of fluo-4 fluorescence from

TABLE 1

Properties of PJF and of spontaneous Ca2+ sparks in WT and MO-injected larvae

Fiber property	WT	Morphant
PJF/JF ratio (mean ± SD)	0.79 ± 0.14[a] ($n = 7$)	0.03 ± 0.03[b] ($n = 10$)
Spark frequency (sarcomere^{-1} s^{-1} (mean ± SEM)	0.083 ± 0.018[c] ($n = 42$)	0.001 ± 0.001[d] ($n = 39$)

For both properties, the morphant values differ from the WT values at $P < 0.01$.

[a]Three experiments, 7 fish, 410 triads from 70 fibers.
[b]Four experiments, 10 fish, 420 triads from 100 fibers.
[c]Four experiments, 42 cells.
[d]Four experiments, 39 cells.

WT and morphant myocytes (left), and longitudinal X-T line scans performed to detect Ca^{2+} sparks (center and right). The bright fluorescent puncta in the XY images are not Ca^{2+} sparks, but rather localized regions of high resting fluorescence that persist with repeated scanning (see figure legend). The frequency with which Ca^{2+} sparks were detected was measured in 42 WT and 39 morphant fibers from four separate experiments and, on average, was found to be much higher in the WT fibers than morphant (0.083 ± 0.018 vs. 0.001 ± 0.001 sarcomere^{-1} s^{-1}; ±SEM; Table 1 and Fig. 4 B, left). About 80% of the morphant fibers had no Ca^{2+} sparks, and spark frequency in the other 20% was low (0.007 ± 0.003 sarcomere^{-1} s^{-1}); in contrast, only ∼12% of WT fibers had no sparks, and spark frequency in the WT fibers ranged as high as 0.61 sarcomere^{-1} s^{-1} (Fig. 4 B, right).

In a separate set of experiments, spark frequencies were compared in fibers derived from WT and MO-tbx5 larvae. The spark frequencies observed in 26 fibers from two separate MO-tbx5 preparations were 0.039 ± 0.017, and those in 16 fibers from two separate WT preparations were 0.039 ± 0.013 sarcomere^{-1} s^{-1} (mean ± SEM). Although the spark frequencies in these last experiments were overall only ∼50% of those measured for the WT fibers associated with the RyR3 MO expression experiments, the difference in the mean values of the

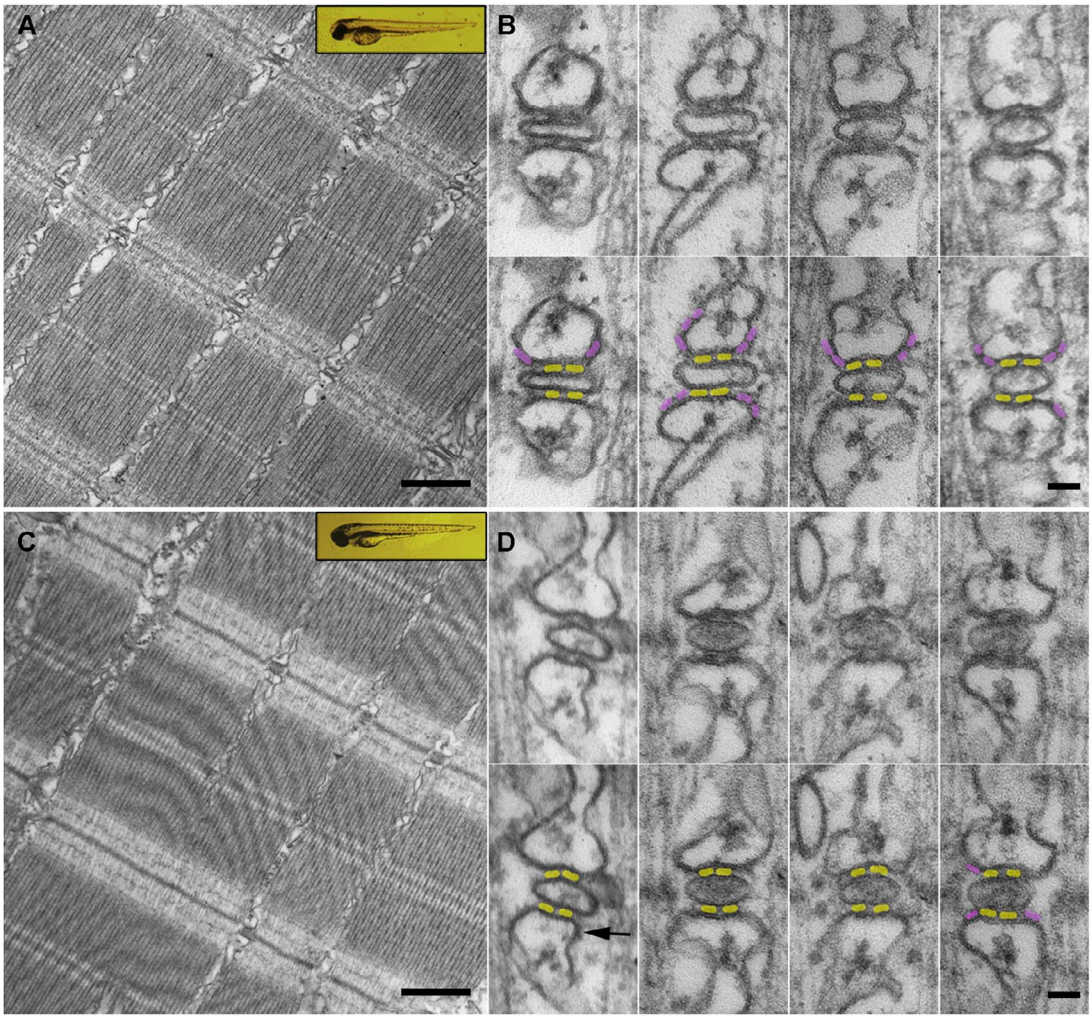

Figure 3. Anatomical effects of the MO injection. Low magnification images and triad details from fibers of WT (A and B) and morphant (C and D) fish. With very few exceptions, the injected fish were not altered either at the level of whole embryo (insets in A and C) or at the overall level of fiber organization (A and C). Bar, 500 nm. However, details of triad structure show that although the frequency of JF is unaltered, PJF are present in WT (B) but missing from the majority of triads in MO-injected fish (D). In B and D, each set of images shows a set of triads above and the same triads below with highlighting of JF (yellow) and PJF (light purple). The four examples in B are characteristic of WT triads. D shows four different examples of morphant triads. In the triad at left one density, indicated by an arrow, is ambiguous. Such ambiguities are rare, and they contribute to the 10% uncertainty in the counts (see Materials and methods). The two triads in the middle represent the large majority of the 420 morphant triads examined, which show no PJF. The triad at right was selected to illustrate one of the rare triads that clearly retained PJF; these were included in the overall counts shown in Table 1. JSR profiles in triads from morphant fish tend to be slightly distorted, possibly because of lower membrane rigidity in the absence of PJF. Other structural variations are not exclusive to morphant fibers. Bar, 50 nm.

two WT datasets is not statistically significant ($P > 0.15$). Overall, the similarity of frequencies in the tbx5 and WT preparations shows that simple injection of an unrelated MO did not affect spark frequencies.

Calcium spark properties

In a subset of the X-T images in which the resting fluorescence intensity was higher than usual, sparks could be detected at a lower $\Delta F/F$ threshold, and the fitted spark properties were more reliable because of the larger signal-to-noise ratio (see Materials and methods). The average frequency of spark detection in these fibers was again much higher in WT compared with morphant (0.125 ± 0.039 sarcomere^{-1} s^{-1}; $n = 23$ fibers vs. 0.004 ± 0.001; $n = 28$ fibers; ±SEM). Averaged X-T images of sparks and spark profiles from these fibers are shown in Fig. 5, and the averaged properties of the individually analyzed sparks are shown in Fig. 6. The sparks detected in morphant fibers are smaller in amplitude, duration, and spatial extent when compared with those in WT fibers. Spark mass (Fig. 6), an estimate of the volume integral of the $\Delta F/F$ signal of an individual spark at its time of peak, which is related to the amount of SR calcium release that gives rise to a spark (Sun et al., 1998; Hollingworth et al., 2001), is about four times smaller in the morphant compared with the WT sparks (0.73 ± 0.17 μm^3, $n = 31$, vs. 3.03 ± 0.19 μm^3, $n = 496$; ±SEM). In contrast, the properties of Ca^{2+} sparks observed in tbx5 MO-injected larvae and those in the associated WT uninjected larvae are indistinguishable ($P > 0.05$ in all six property tests; not depicted).

72 hpf zebrafish larvae swimming behavior is unaltered by RyR3 silencing

To assess the functional effect of RyR3 silencing on EC coupling at a macroscopic level, we analyzed swimming

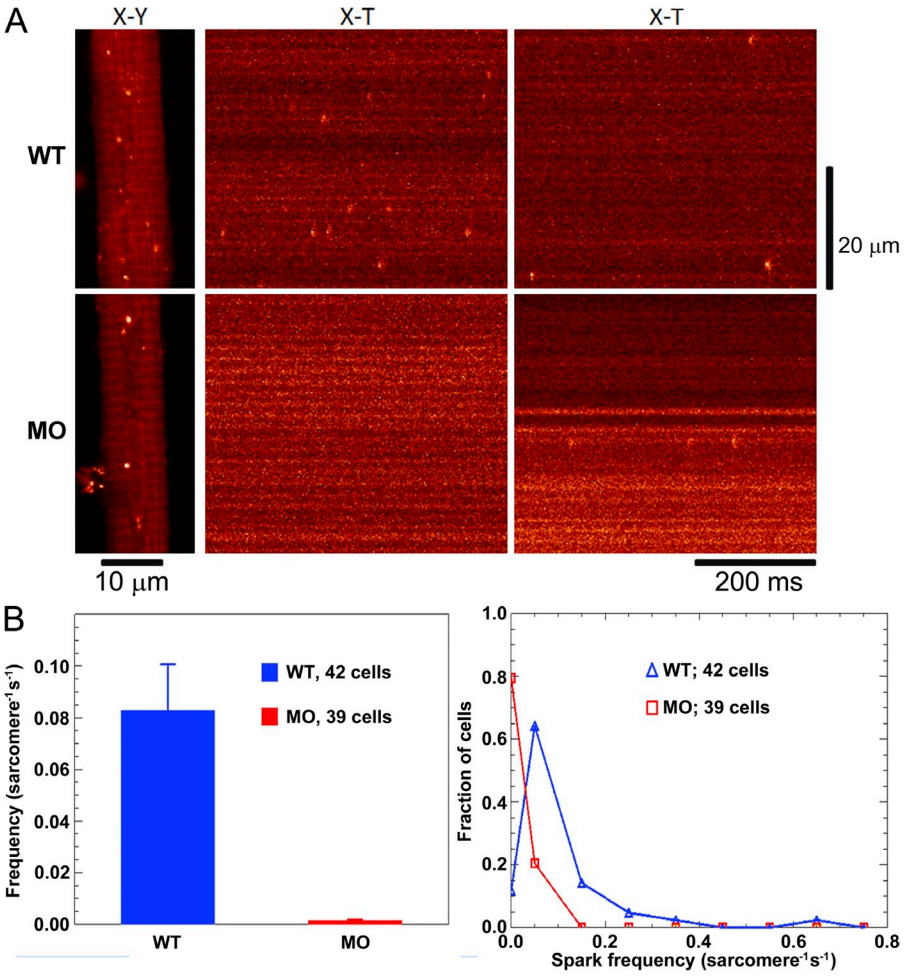

Figure 4. Comparison of calcium sparks in WT and MO preparations. (A) Confocal images of fluo-4 AM–loaded myocytes isolated, the same day, from 72 hpf WT and MO-injected larvae. The bathing solution included 0.3 mM caffeine to stimulate SR calcium release. (Left) X-Y images. The bright puncta in these images are not Ca^{2+} sparks but localized regions of high resting fluorescence that persist with repeated scanning. These bright puncta may arise from fluo-4 molecules contained within a small organelle with elevated free [Ca^{2+}] (Hollingworth et al., 2001). (Middle and right) X-T images from longitudinal line scans of the myocytes. The horizontal banding pattern in the X-Y and X-T images likely arises from binding of the dye to sarcomeric structures, here spaced at distances close to 1.85 μm. Ca^{2+} sparks are the brief, spatially localized increases in fluorescence (bright orange) that are clearly seen in the WT X-T images; they vary in frequency from cell to cell. The bottom right panel shows sparks from one of the few sparking MO cells. (B, left) Mean spark frequency measured in 42 WT and 39 morphant cells from four separate experiments of each type. (Right) The distribution of spark frequency in the WT and morphant cells. For frequencies above 0, the symbols are plotted at the center frequency of bin widths of 0.1 sarcomere^{-1} s^{-1}. In the case of the morphant cells, sparks were sufficiently rare that the mean value of the frequencies in the first bin is 0.0065 ± 0.0028 sarcomere^{-1} s^{-1} ($n = 8$; ±SEM), considerably less than the position of the central frequency (0.05 sarcomere^{-1} s^{-1}).

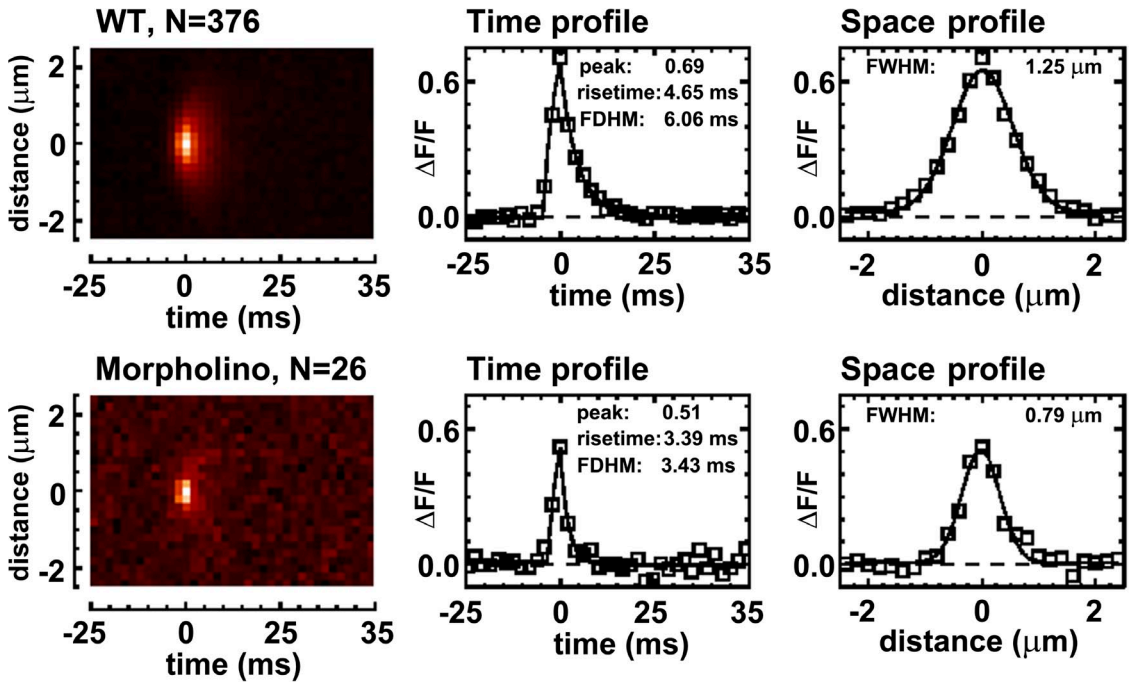

Figure 5. Comparison of average sparks in WT and MO preparations. (Left) Averaged line-scan images of Ca^{2+} sparks with peak amplitude >0.5 ΔF/F, detected in WT (top) and morphant (bottom) preparations. Time and space profiles obtained from these average sparks are shown (middle and right, squares) along with the best fits of standard waveforms to these profiles (curves; see Materials and methods). Labels give spark parameters obtained from these fits; FDHM, full duration of the time profile at half-maximum amplitude. The sparks from morphant cells are smaller, briefer, and narrower than those from WT cells.

movements of MO-injected and uninjected sibling larvae at 72 hpf using a high speed camera. At this time point, the swimbladder is not yet inflated, so to maintain the larvae in an upright position for effective analysis of tail movements, larvae were partially restrained by embedding the heads in agarose, leaving the tails free to move. Because spontaneous movements are infrequent at this age, we induced tail flips by providing a gentle tactile stimulus to the tail (Fig. 7 A, representative images). We performed a detailed analysis of tail movements by imaging at 1,000 Hz and using automated tracking software to determine the kinematics of each response (Burgess and Granato, 2007a,b; Wolman et al., 2011). Morphant and control larvae were equally responsive to tactile stimuli (not depicted). To analyze tail movements, the body of each larva was subdivided into four segments

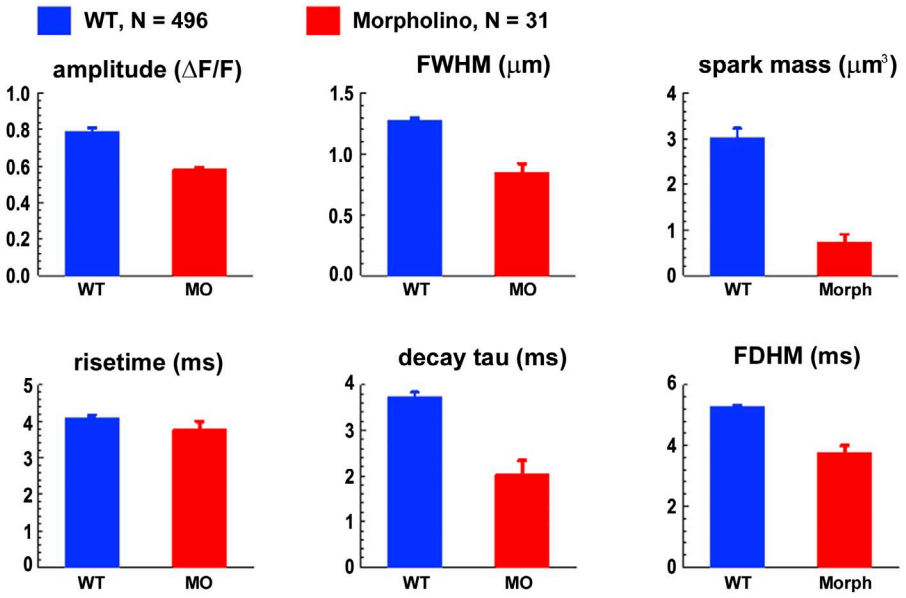

Figure 6. Properties (mean ± SEM) of the individually analyzed sparks with peak amplitude >0.5 ΔF/F, detected in WT (blue) and morphant (red) myocytes. Spark mass (Hollingworth et al., 2001), an estimate of the volume integral of ΔF/F at the time of spark peak, is related to the amount of calcium released. The numbers of sparks analyzed individually (496 and 31) are larger than the numbers of sparks averaged for the images in Fig. 5 (376 and 26) because sparks were included in the averaged images only if the full time and space ranges were recorded and were free of other spark activity. All properties except for rise time are significantly different between WT and MO at $P < 0.01$.

(indicated by color lines over the larva in Fig. 7 A, top left), and the angles between segments were measured for each time point. Because of the head-restrained mounting, the primary movement involved segments 2, 3, and 4, and thus, to calculate the tail curvature, we took the sum of the angles between segments 2 and 3 and segments 3 and 4 (Fig. 7 B, representative traces). Maximum tail curvature, mean bend magnitude (change in curvature), maximum angular velocity, tail bend frequency, and total number of bends per response were calculated (Fig. 7 C; mean ± SEM, $n = 10$ responses from three control fish and $n = 27$ responses from six morphant fish). None of these parameters was significantly different ($P > 0.25$, Student's t test) between morphants and controls, indicating that RyR3 and PJF are not essential for normal movement of the tail at 72 hpf.

DISCUSSION

The rapid embryonic development of zebrafish is one of the reasons why this animal model has become so popular in various biological disciplines, including physiology and developmental biology. We observed the presence of fully formed muscle fibers with well-aligned striations and perfectly located triads in zebrafish larvae tail myotomes as early as 48 hpf (Fig. 1; see also Schredelseker et al., 2005). This provides an essential time frame for our experiments, as the MO-silencing effect can be trusted to last up to 72 hpf. At 72 hpf, PJF are clearly detectable in WT fast-twitch muscle fibers, which constitute the bulk of the tail myotomes, allowing us to follow and confirm the specificity and the effectiveness of the RyR3-targeted MO. In WT animals, the ratio of PJF to JF is comparable to that found in frog fibers and considerably more elevated than that in adult or even embryonic mammalian muscle (Felder and Franzini-Armstrong, 2002). In morphant larvae, as in WT larvae, the two rows of JF are visible in all triads, confirming the unaltered expression and appropriate positioning of RyR1 in the morphants (Fig. 3). In contrast, PJF are essentially missing in the morphant larvae, directly confirming that PJF are constituted of RyR3. No other abnormality is detected in the ultrastructure of morphants, highlighting the specificity of the effect as well as the fact that RyR3s are not essential for muscle differentiation, as already suggested by the result of a null mutation for RyR3 in mouse (Barone et al., 1998).

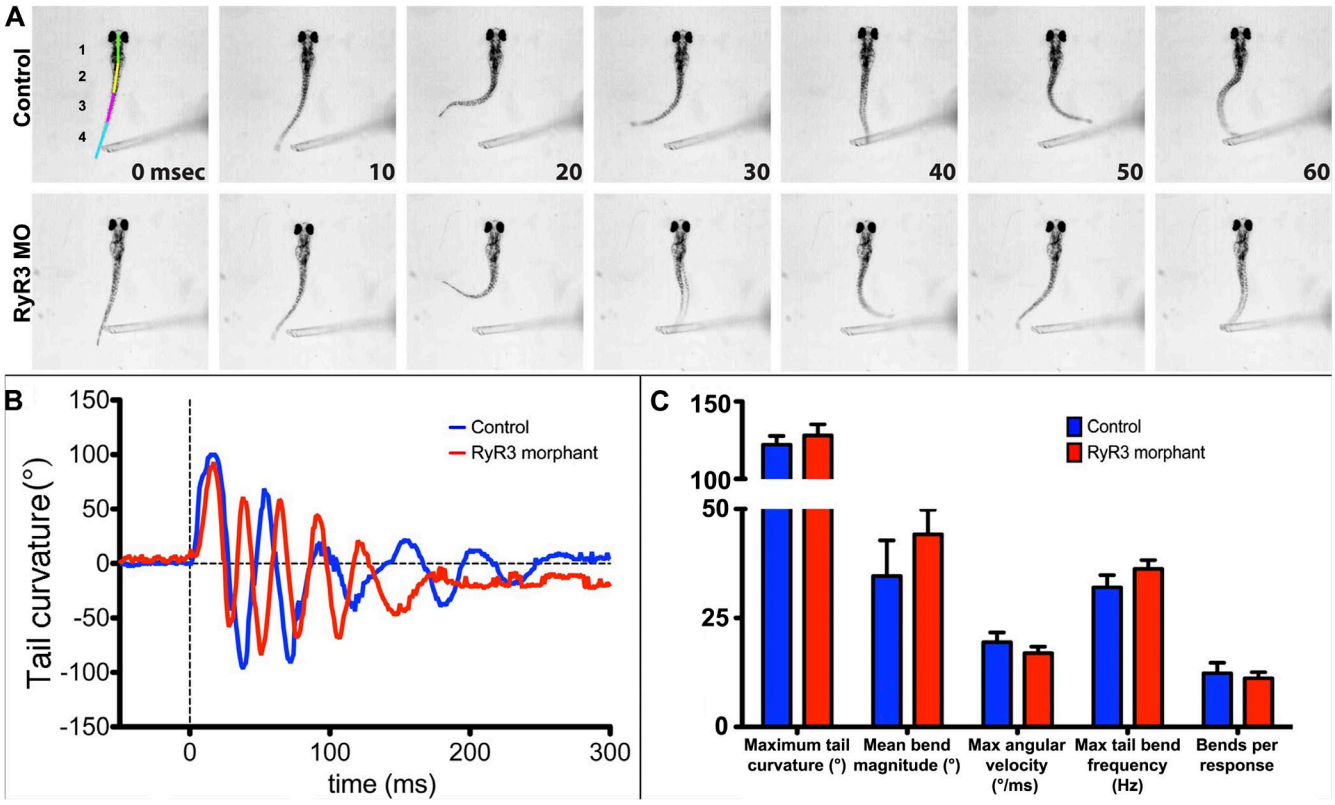

Figure 7. High speed video recording of touch-induced tail flips in 72 hpf larvae at room temperature. The head was immobilized in agar, keeping the tail free to move. Representative images (A) in each row are separated by 10 ms, with the colored lines (top left) indicating the body segments used for kinematic analysis. Neither the tail curvature plots (B, representative plot) nor any other movement parameters (C) indicate any clear differences in the stimulus-activated responses of WT and morphant tails.

Fibers from tails of WT zebrafish produce readily detected brief local Ca^{2+} releases (Ca^{2+} sparks) under the effect of a low concentration of caffeine (0.3 mM). Under identical conditions, morphant fibers that lack PJF but have a full complement of JF are almost silent (Fig. 4). This is not because of calcium depletion in the morphant fibers, as morphant tails respond to stimuli as effectively as WT (Fig. 7). Because, as detailed above, there is no reason to expect that the two sets of fibers differ in anything besides the presence or absence of RyR3, the experiments provide strong evidence that the recorded sparks require the activity of RyR3. A relationship, between the presence of readily detectable Ca^{2+} sparks and the presence of a detectable amount of RyR3, was first observed in comparisons of spark behavior in fibers from adult frog muscle, which have RyR3, and fibers from adult rat muscle, which do not (Shirokova et al., 1998). The relationship was partly confirmed by overexpression of RyR3 in adult mouse fibers (Pouvreau et al., 2007) and is strengthened in the current study, which compared, under identical experimental conditions, the effect of RyR3 presence and absence in fibers at the same age from the same species and with the same complement and location of RyR1.

The sparks detected in WT zebrafish fibers (Figs. 5 and 6) have morphological properties similar to those reported in intact frog fibers imaged on the same microscope; the latter sparks were observed at low frequency in resting fibers and at higher frequency in fibers depolarized by 8–13 mM of extracellular $[K^+]$ (Hollingworth et al., 2006). This similarity is consistent with the comparable numbers of PJF observed in the two sets of muscles, which also have a common location of their triads, at the Z-line. One detectable difference in spark morphological properties is in the full width at half-maximum, which is 0.99 ± 0.01 μm (±SEM) in frog fibers and 1.28 ± 0.02 μm in WT zebrafish fibers. This difference might arise because of fiber differences, such as the concentrations of Ca^{2+}-binding constituents in myoplasm and/or experimental differences, such as (a) the method used to activate sparks (K^+ depolarization in frog fibers, 0.3 mM caffeine in zebrafish fibers) or (b) the Ca^{2+} indicator used to detect sparks (microinjection of membrane-impermeant fluo-3 in frog, AM loading of fluo-4 in zebrafish).

Analysis of the frog sparks described above suggests that the underlying SR Ca^{2+} release flux was caused by two to four active RyRs (Hollingworth et al., 2006). This number could be larger in zebrafish given that spark mass (a property of individual sparks) is larger with zebrafish sparks, 3.03 ± 0.19 μm^3 (see Results) compared with frog sparks, 1.21 ± 0.04 μm^3 (Hollingworth et al., 2006). Our observation here, that spark mass is reduced about fourfold with silencing of RyR3 expression (Fig. 6), suggests that the majority of the Ca^{2+} release flux underlying a WT spark in zebrafish fibers comes through RyR3. We do not know whether the very few and smaller sparks that can still be detected in RyR3-silenced fibers arise because (a) the expression of RyR3 is not 100% inhibited by the MO (an observation consistent with the presence of a few remaining PJF in the morphant fibers; Table 1) or (b) the sparks arise from activity in RyR1 only. Also unknown is whether a caffeine-activated spark is initiated by the opening of RyR1 or RyR3. It is clear, however, that the RyR3s provide the major source of Ca^{2+} for the sparks observed in WT fibers.

The unaltered swimming behavior of morphant larvae (Fig. 7) suggests that, in WT fibers, the dominant contribution of RyR3 to Ca^{2+} release during a spark does not apply to the Ca^{2+} release initiated by action-potential stimuli because, if it did, the morphant larvae would likely have had a substantial reduction in their tail-flip response. Thus, the Ca^{2+} release flux in response to an action potential in WT fibers does not appear to be a simple summation of the release events that underlie Ca^{2+} sparks; rather, with an action potential, the fractional contribution of Ca^{2+} release through RyR3s is probably reduced. The likely explanation is that, with an action potential, many RyR1s will be activated nearly simultaneously throughout the fiber volume, and the resultant rise in free $[Ca^{2+}]$ will induce a rapid and powerful Ca^{2+}-dependent inactivation of the Ca^{2+} release system. This inactivation mechanism is observed in amphibian twitch fibers (Baylor and Hollingworth, 1988; Schneider and Simon, 1988; Jong et al., 1995), mammalian fast-twitch and slow-twitch fibers (Hollingworth et al., 1996; Baylor and Hollingworth, 2003), and toadfish superfast fibers (Rome et al., 1996). For example, in frog fibers stimulated by an action potential, 90% or more of the RyRs are inactivated within a few milliseconds (14–15°C), and it is likely that many RyRs are already inactivated at the peak of the release flux (Jong et al., 1995). Because, with an action potential, activation of RyR3s is thought to depend on prior activation of RyR1s, the fractional contribution of RyR3s to the release flux might then be preferentially suppressed by inactivation. Consistent with this possibility, simulations of the action potential–evoked Ca^{2+} transient in (adult) frog fibers reveal a delayed component of release that is not present in (adult) mammalian fibers (Hollingworth and Baylor, 2013). This component, which is estimated to account for only ∼20% of the total release in frog fibers, is suggested to be caused by RyR3, with the majority of the release, ∼80%, caused by RyR1.

The authors wish to thank Dr. Klara Pendrak for help provided in the Western blotting analysis.

This work was supported by National Institutes of Health grants RO1 HL 48093 (to C. Franzini-Armstrong) and 2PO1 AR052354 P.D. Allen (PI) Core D (to C. Franzini-Armstrong), and National Research Service Award 1F32NS077815-01 (to K.C. Marsden).

The authors declare no competing financial interests.

Eduardo Rios served as editor.

Submitted: 13 October 2014
Accepted: 15 January 2015

REFERENCES

Airey, J.A., C.F. Beck, K. Murakami, S.J. Tanksley, T.J. Deerinck, M.H. Ellisman, and J.L. Sutko. 1990. Identification and localization of two triad junctional foot protein isoforms in mature avian fast twitch skeletal muscle. *J. Biol. Chem.* 265:14187–14194.

Barone, V., F. Bertocchini, R. Bottinelli, F. Protasi, P.D. Allen, C. Franzini Armstrong, C. Reggiani, and V. Sorrentino. 1998. Contractile impairment and structural alterations of skeletal muscles from knockout mice lacking type 1 and type 3 ryanodine receptors. *FEBS Lett.* 422:160–164. http://dx.doi.org/10.1016/S0014-5793(98)00003-9

Baylor, S.M., and S. Hollingworth. 1988. Fura-2 calcium transients in frog skeletal muscle fibres. *J. Physiol.* 403:151–192. http://dx.doi.org/10.1113/jphysiol.1988.sp017244

Baylor, S.M., and S. Hollingworth. 2003. Sarcoplasmic reticulum calcium release compared in slow-twitch and fast-twitch fibres of mouse muscle. *J. Physiol.* 551:125–138. http://dx.doi.org/10.1113/jphysiol.2003.041608

Block, B.A., T. Imagawa, K.P. Campbell, and C. Franzini-Armstrong. 1988. Structural evidence for direct interaction between the molecular components of the transverse tubule/sarcoplasmic reticulum junction in skeletal muscle. *J. Cell Biol.* 107:2587–2600. http://dx.doi.org/10.1083/jcb.107.6.2587

Burgess, H.A., and M. Granato. 2007a. Modulation of locomotor activity in larval zebrafish during light adaptation. *J. Exp. Biol.* 210:2526–2539. http://dx.doi.org/10.1242/jeb.003939

Burgess, H.A., and M. Granato. 2007b. Sensorimotor gating in larval zebrafish. *J. Neurosci.* 27:4984–4994. http://dx.doi.org/10.1523/JNEUROSCI.0615-07.2007

Burgess, H.A., S.L. Johnson, and M. Granato. 2009. Unidirectional startle responses and disrupted left-right co-ordination of motor behaviors in robo3 mutant zebrafish. *Genes Brain Behav.* 8:500–511. http://dx.doi.org/10.1111/j.1601-183X.2009.00499.x

Conklin, M.W., V. Barone, V. Sorrentino, and R. Coronado. 1999. Contribution of ryanodine receptor type 3 to Ca^{2+} sparks in embryonic mouse skeletal muscle. *Biophys. J.* 77:1394–1403. http://dx.doi.org/10.1016/S0006-3495(99)76988-2

Conklin, M.W., C.A. Ahern, P. Vallejo, V. Sorrentino, H. Takeshima, and R. Coronado. 2000. Comparison of Ca^{2+} sparks produced independently by two ryanodine receptor isoforms (type 1 or type 3). *Biophys. J.* 78:1777–1785. http://dx.doi.org/10.1016/S0006-3495(00)76728-2

Darbandi, S., and J.P. Franck. 2009. A comparative study of ryanodine receptor (RyR) gene expression levels in a basal ray-finned fish, bichir (*Polypterus ornatipinnis*) and the derived euteleost zebrafish (*Danio rerio*). *Comp. Biochem. Physiol. B Biochem. Mol. Biol.* 154:443–448. http://dx.doi.org/10.1016/j.cbpb.2009.09.003

Devoto, S.H., E. Melançon, J.S. Eisen, and M. Westerfield. 1996. Identification of separate slow and fast muscle precursor cells in vivo, prior to somite formation. *Development.* 122:3371–3380.

Elworthy, S., M. Hargrave, R. Knight, K. Mebus, and P.W. Ingham. 2008. Expression of multiple slow myosin heavy chain genes reveals a diversity of zebrafish slow twitch muscle fibres with differing requirements for Hedgehog and Prdm1 activity. *Development.* 135:2115–2126. http://dx.doi.org/10.1242/dev.015719

Felder, E., and C. Franzini-Armstrong. 2002. Type 3 ryanodine receptors of skeletal muscle are segregated in a parajunctional position. *Proc. Natl. Acad. Sci. USA.* 99:1695–1700. http://dx.doi.org/10.1073/pnas.032657599

Franck, J.P., J. Morrissette, J.E. Keen, R.L. Londraville, M. Beamsley, and B.A. Block. 1998. Cloning and characterization of fiber type-specific ryanodine receptor isoforms in skeletal muscles of fish. *Am. J. Physiol.* 275:C401–C415.

Giannini, G., A. Conti, S. Mammarella, M. Scrobogna, and V. Sorrentino. 1995. The ryanodine receptor/calcium channel genes are widely and differentially expressed in murine brain and peripheral tissues. *J. Cell Biol.* 128:893–904. http://dx.doi.org/10.1083/jcb.128.5.893

Hakamata, Y., J. Nakai, H. Takeshima, and K. Imoto. 1992. Primary structure and distribution of a novel ryanodine receptor/calcium release channel from rabbit brain. *FEBS Lett.* 312:229–235. http://dx.doi.org/10.1016/0014-5793(92)80941-9

Hollingworth, S., and S.M. Baylor. 2013. Comparison of myoplasmic calcium movements during excitation–contraction coupling in frog twitch and mouse fast-twitch muscle fibers. *J. Gen. Physiol.* 141:567–583. http://dx.doi.org/10.1085/jgp.201310961

Hollingworth, S., M. Zhao, and S.M. Baylor. 1996. The amplitude and time course of the myoplasmic free $[Ca^{2+}]$ transient in fast-twitch fibers of mouse muscle. *J. Gen. Physiol.* 108:455–469. http://dx.doi.org/10.1085/jgp.108.5.455

Hollingworth, S., J. Peet, W.K. Chandler, and S.M. Baylor. 2001. Calcium sparks in intact skeletal muscle fibers of the frog. *J. Gen. Physiol.* 118:653–678. http://dx.doi.org/10.1085/jgp.118.6.653

Hollingworth, S., W.K. Chandler, and S.M. Baylor. 2006. Effects of tetracaine on voltage-activated calcium sparks in frog intact skeletal muscle fibers. *J. Gen. Physiol.* 127:291–307. http://dx.doi.org/10.1085/jgp.200509477

Ivanenko, A., D.D. McKemy, J.L. Kenyon, J.A. Airey, and J.L. Sutko. 1995. Embryonic chicken skeletal muscle cells fail to develop normal excitation-contraction coupling in the absence of the alpha ryanodine receptor. Implications for a two-ryanodine receptor system. *J. Biol. Chem.* 270:4220–4223. http://dx.doi.org/10.1074/jbc.270.9.4220

Jong, D.S., P.C. Pape, S.M. Baylor, and W.K. Chandler. 1995. Calcium inactivation of calcium release in frog cut muscle fibers that contain millimolar EGTA or Fura-2. *J. Gen. Physiol.* 106:337–388. http://dx.doi.org/10.1085/jgp.106.2.337

Kirsch, W.G., D. Uttenweiler, and R.H. Fink. 2001. Spark- and ember-like elementary Ca^{2+} release events in skinned fibres of adult mammalian skeletal muscle. *J. Physiol.* 537:379–389. http://dx.doi.org/10.1111/j.1469-7793.2001.00379.x

Klein, M.G., H. Cheng, L.F. Santana, Y.H. Jiang, W.J. Lederer, and M.F. Schneider. 1996. Two mechanisms of quantized calcium release in skeletal muscle. *Nature.* 379:455–458. http://dx.doi.org/10.1038/379455a0

Lacampagne, A., C.W. Ward, M.G. Klein, and M.F. Schneider. 1999. Time course of individual Ca^{2+} sparks in frog skeletal muscle recorded at high time resolution. *J. Gen. Physiol.* 113:187–198. http://dx.doi.org/10.1085/jgp.113.2.187

Lai, F.A., H.P. Erickson, E. Rousseau, Q.Y. Liu, and G. Meissner. 1988. Purification and reconstitution of the calcium release channel from skeletal muscle. *Nature.* 331:315–319. http://dx.doi.org/10.1038/331315a0

Legrand, C., E. Giacomello, C. Berthier, B. Allard, V. Sorrentino, and V. Jacquemond. 2008. Spontaneous and voltage-activated Ca^{2+} release in adult mouse skeletal muscle fibres expressing the type 3 ryanodine receptor. *J. Physiol.* 586:441–457. http://dx.doi.org/10.1113/jphysiol.2007.145862

Moore, R.A., H. Nguyen, J. Galceran, I.N. Pessah, and P.D. Allen. 1998. A transgenic myogenic cell line lacking ryanodine receptor protein for homologous expression studies: Reconstitution of

Ry_1R protein and function. *J. Cell Biol.* 140:843–851. http://dx.doi.org/10.1083/jcb.140.4.843

Murayama, T., and Y. Ogawa. 1992. Purification and characterization of two ryanodine-binding protein isoforms from sarcoplasmic reticulum of bullfrog skeletal muscle. *J. Biochem.* 112:514–522.

Nakai, J., R.T. Dirksen, H.T. Nguyen, I.N. Pessah, K.G. Beam, and P.D. Allen. 1996. Enhanced dihydropyridine receptor channel activity in the presence of ryanodine receptor. *Nature.* 380:72–75. http://dx.doi.org/10.1038/380072a0

O'Brien, J., G. Meissner, and B.A. Block. 1993. The fastest contracting muscles of nonmammalian vertebrates express only one isoform of the ryanodine receptor. *Biophys. J.* 65:2418–2427. http://dx.doi.org/10.1016/S0006-3495(93)81303-1

Ogawa, Y., N. Kurebayashi, and T. Murayama. 2000. Putative roles of type 3 ryanodine receptor isoforms (RyR3). *Trends Cardiovasc. Med.* 10:65–70. http://dx.doi.org/10.1016/S1050-1738(00)00050-5

Percival, A.L., A.J. Williams, J.L. Kenyon, M.M. Grinsell, J.A. Airey, and J.L. Sutko. 1994. Chicken skeletal muscle ryanodine receptor isoforms: ion channel properties. *Biophys. J.* 67:1834–1850. http://dx.doi.org/10.1016/S0006-3495(94)80665-4

Pouvreau, S., L. Royer, J. Yi, G. Brum, G. Meissner, E. Ríos, and J. Zhou. 2007. Ca^{2+} sparks operated by membrane depolarization require isoform 3 ryanodine receptor channels in skeletal muscle. *Proc. Natl. Acad. Sci. USA.* 104:5235–5240. http://dx.doi.org/10.1073/pnas.0700748104

Protasi, F., C. Franzini-Armstrong, and P.D. Allen. 1998. Role of ryanodine receptors in the assembly of calcium release units in skeletal muscle. *J. Cell Biol.* 140:831–842. http://dx.doi.org/10.1083/jcb.140.4.831

Protasi, F., H. Takekura, Y. Wang, S.R. Chen, G. Meissner, P.D. Allen, and C. Franzini-Armstrong. 2000. RYR1 and RYR3 have different roles in the assembly of calcium release units of skeletal muscle. *Biophys. J.* 79:2494–2508. http://dx.doi.org/10.1016/S0006-3495(00)76491-5

Rome, L.C., D.A. Syme, S. Hollingworth, S.L. Lindstedt, and S.M. Baylor. 1996. The whistle and the rattle: the design of sound producing muscles. *Proc. Natl. Acad. Sci. USA.* 93:8095–8100. http://dx.doi.org/10.1073/pnas.93.15.8095

Schneider, M.F., and B.J. Simon. 1988. Inactivation of calcium release from the sarcoplasmic reticulum in frog skeletal muscle. *J. Physiol.* 405:727–745. http://dx.doi.org/10.1113/jphysiol.1988.sp017358

Schredelseker, J., V. Di Biase, G.J. Obermair, E.T. Felder, B.E. Flucher, C. Franzini-Armstrong, and M. Grabner. 2005. The beta 1a subunit is essential for the assembly of dihydropyridine-receptor arrays in skeletal muscle. *Proc. Natl. Acad. Sci. USA.* 102:17219–17224. http://dx.doi.org/10.1073/pnas.0508710102

Shirokova, N., J. García, and E. Ríos. 1998. Local calcium release in mammalian skeletal muscle. *J. Physiol.* 512:377–384. http://dx.doi.org/10.1111/j.1469-7793.1998.377be.x

Shirokova, N., R. Shirokov, D. Rossi, A. González, W.G. Kirsch, J. García, V. Sorrentino, and E. Ríos. 1999. Spatially segregated control of Ca^{2+} release in developing skeletal muscle of mice. *J. Physiol.* 521:483–495. http://dx.doi.org/10.1111/j.1469-7793.1999.00483.x

Sun, X.P., N. Callamaras, J.S. Marchant, and I. Parker. 1998. A continuum of InsP3-mediated elementary Ca^{2+} signalling events in *Xenopus* oocytes. *J. Physiol.* 509:67–80. http://dx.doi.org/10.1111/j.1469-7793.1998.067bo.x

Takekura, H., M. Nishi, T. Noda, H. Takeshima, and C. Franzini-Armstrong. 1995. Abnormal junctions between surface membrane and sarcoplasmic reticulum in skeletal muscle with a mutation targeted to the ryanodine receptor. *Proc. Natl. Acad. Sci. USA.* 92:3381–3385. http://dx.doi.org/10.1073/pnas.92.8.3381

Takeshima, H., M. Iino, H. Takekura, M. Nishi, J. Kuno, O. Minowa, H. Takano, and T. Noda. 1994. Excitation-contraction uncoupling and muscular degeneration in mice lacking functional skeletal muscle ryanodine-receptor gene. *Nature.* 369:556–559. http://dx.doi.org/10.1038/369556a0

Tamura, K., S. Yonei-Tamura, and J.C. Izpisúa Belmonte. 1999. Differential expression of Tbx4 and Tbx5 in Zebrafish fin buds. *Mech. Dev.* 87:181–184. http://dx.doi.org/10.1016/S0925-4773(99)00126-4

Tsugorka, A., E. Ríos, and L.A. Blatter. 1995. Imaging elementary events of calcium release in skeletal muscle cells. *Science.* 269:1723–1726. http://dx.doi.org/10.1126/science.7569901

Wang, X., N. Weisleder, C. Collet, J. Zhou, Y. Chu, Y. Hirata, X. Zhao, Z. Pan, M. Brotto, H. Cheng, and J. Ma. 2005. Uncontrolled calcium sparks act as a dystrophic signal for mammalian skeletal muscle. *Nat. Cell Biol.* 7:525–530. http://dx.doi.org/10.1038/ncb1254

Ward, C.W., F. Protasi, D. Castillo, Y. Wang, S.R. Chen, I.N. Pessah, P.D. Allen, and M.F. Schneider. 2001. Type 1 and type 3 ryanodine receptors generate different Ca^{2+} release event activity in both intact and permeabilized myotubes. *Biophys. J.* 81:3216–3230. http://dx.doi.org/10.1016/S0006-3495(01)75957-7

Wolman, M.A., R.A. Jain, L. Liss, and M. Granato. 2011. Chemical modulation of memory formation in larval zebrafish. *Proc. Natl. Acad. Sci. USA.* 108:15468–15473. http://dx.doi.org/10.1073/pnas.1107156108

Wu, H.H., C. Brennan, and R. Ashworth. 2011. Ryanodine receptors, a family of intracellular calcium ion channels, are expressed throughout early vertebrate development. *BMC Res. Notes.* 4:541. http://dx.doi.org/10.1186/1756-0500-4-541